Supplementary Information for

Ordered mesoporous porphyrinic carbons with very high electrocatalytic activity for the oxygen reduction reaction

Jae Yeong Cheon[1], Taeyoung Kim[2], YongMan Choi[3], Hu Young Jeong[4,5], Min Gyu Kim[6], Young Jin Sa[1], Jaesik Kim[1], Zonghoon Lee[5], Tae-Hyun Yang[2], Kyungjung Kwon[7], Osamu Terasaki[8,9], Gu-Gon Park[2*], Radoslav R. Adzic[10*], and Sang Hoon Joo[1*]

[1]Department of Chemistry, School of Nano-Bioscience and Chemical Engineering, KIER-UNIST Advanced Center for Energy, and Low-Dimensional Carbon Materials Center, Ulsan National Institute of Science and Technology (UNIST), 50 UNIST-gil, Ulsan 689-798, Republic of Korea
[2]Fuel Cell Research Center, Korea Institute of Energy Research (KIER), 152 Gajeongro, Daejeon 305-343, Republic of Korea
[3]SABIC Technology Center, Riyadh 11551, Saudi Arabia
[4]UNIST Central Research Facility, UNIST, 50 UNIST-gil, Ulsan 689-798, Republic of Korea
[5]School of Mechanical and Advanced Materials Engineering, UNIST, 50 UNIST-gil, Ulsan 689-798, Republic of Korea
[6]Beamline Research Division, Pohang Accelerator Laboratory (PAL), Pohang 790-784, Republic of Korea
[7]Department of Energy & Mineral Resources Engineering, Sejong University, Seoul 143-747, Republic of Korea
[8]Graduate School of EEWS (WCU), Korea Advanced Institute of Science and Technology, 335 Gwahangno, Yuseong-Gu, Daejeon 305-701, Republic of Korea
[9]Department of Materials and Environmental Chemistry, Berzelii center EXSELENT on Porous Materials, Stockholm University, S-10691, Sweden.
[10]Chemistry Department, Brookhaven National Laboratory, Building 555, Upton, New York 11973-5000, USA.

*e-mail: shjoo@unist.ac.kr; adzic@bnl.gov; gugon@kier.re.kr

1. Material Synthesis

Synthesis of OMS templates

Hexagonally ordered mesoporous silica SBA-15 was synthesized following the previously described method[S1], except that the hydrothermal temperature was modified. Pluronic® P123 (8.0 g, M_w = 5800, Aldrich), deionized (DI) water (251.4 g), and 35% HCl (48.6 g, 35 wt%, Samchun) were added to a 500 mL polypropylene bottle, and the mixture was stirred at 35 °C. After P123 was completely dissolved, tetraethyl orthosilicate (17.0 g, 98%, Aldrich) was added and the solution was stirred again for 5 min and then aged at 35 °C without stirring for 24 h. The reaction mixture was then transferred to a Teflon®-lined autoclave and heated at 150 °C for 24 h. The resulting white-coloured precipitates were filtered and washed twice with DI water, and then dried in an oven at 60 °C for 1 d. Finally, the dried sample was calcined at 550 °C for 5 h in air.

Large pore mesoporous silica MSU-F was synthesized following the literature method[S2]. Pluronic® P123 (8.4 g) and DI water (336.8 g) were added to a 500 mL polypropylene bottle, and the mixture was stirred at 35 °C. After P123 was completely dissolved, mesitylene (4.2 g, 98%, Aldrich) was added and the solution was stirred again for 1 h at 35 °C. Sodium silicate solution (20.6 g, ~26.5% SiO_2, Aldrich) and 10% acetic acid (43.7 g, 99.7 wt%, Junsei) were sequentially added, and the solution was aged at 35 °C with stirring for 20 h. The reaction mixture was then transferred to a Teflon®-lined autoclave and heated at 100 °C for 24 h. Subsequent washing and calcination were carried out in the same manner described above for SBA-15.

Cubic *Ia3d* mesoporous silica KIT-6 was synthesized following the previously reported method[S3]. Pluronic® P123 (7.0 g), DI water (250 g), and 35% HCl (13.5 g) were added to a 500 mL polypropylene bottle, and the mixture was stirred at 30 °C. After P123 was completely dissolved, butanol (8.94 g, 99.4%, Aldrich) was added to the solution. After 1 h of stirring, tetraethyl orthosilicate (22.2 g) was added and the solution was stirred for 24 h at 30 °C, and subsequently heated for 24 h at 100 °C under static conditions. Subsequent washing and calcination were carried out in the same manner described above for SBA-15.

Synthesis of FeCo-KB Catalyst

Carbon black (Ketjenblack® 300) was mixed with a 1:1 (in mass ratio) precursor mixture of FeTMPPCl and CoTMPP, pyrolysed at 800 °C under N_2 flow, and finally washed with 0.5 M H_2SO_4 at 80 °C for 8 h. The Fe and Co loadings in the FeCo-KB catalyst were 1.7 and 1.2 %, respectively, which were similar to the metal loadings in the FeCo-OMPC catalyst.

Synthesis of FeCo-Carbosil Catalyst

Fumed silica (Cab-O-sil® M-5, Fluka) was mixed with a 1:1 (in mass ratio) precursor mixture of FeTMPPCl and CoTMPP, pyrolysed at 800 °C under N_2 flow. The silica was leached out by the same procedure as described for M-OMPC catalysts.

2. Characterisation methods

X-ray diffraction (XRD) patterns of the samples were measured with an X-ray diffractometer (Rigaku D/Max 2500V/PC) equipped with a Cu Kα source operating at 40 kV and 200 mA. The morphologies of the samples were observed using a scanning electron microscope (SEM) (Quanta 200, FEI) operating at 18 kV. The microstructural and elemental

analyses of the catalyst powders were performed using HRTEM, HAADF-STEM [JEOL JEM 2100F with a probe forming Cs corrector at 200 kV (convergence angle: 30 mrad, semi-angles for HAADF detector: 61–163 mrad)], and EELS techniques (FEI Titan^3 G2 cube 60-300 with an image forming Cs corrector equipped with a monochromator). EELS spectra were collected using a Gatan Quantum 965 spectrometer where a monochromated electron beam was excited. The porous structures of the samples were analysed by a nitrogen adsorption experiment at −196 °C using a BEL BELSORP-Max system. The surface areas of the samples were calculated using the Brunauer-Emmett-Teller (BET) equation. The mesopore and micropore size distributions of the samples were calculated using the Barrett-Joyner-Halenda (BJH) and the Horvath-Kawazoe (HK) algorithms, respectively. The surface compositions of the catalysts were measured using an X-ray photoelectron spectrometer (XPS) (K-Alpha, Thermo Scientific), equipped with a monochromatic Al K-α X-ray source (1486.6 eV). Individual chemical components of the N 1s binding energy (BE) region were fitted to the spectra by the Gaussian (Gaussian 70, Lorentzian 30)-function after a linear (Shirley)-type background subtraction. The carbon, hydrogen, and nitrogen contents in the samples were determined by Thermo Scientific Flash 2000 elemental analyser. The metal contents in the catalysts were measured by inductively coupled plasma optical emission spectrometry (ICP-OES) using a Varian 720-ES instrument.

3. X-ray absorption spectroscopy

Fe and Co K-edge X-ray absorption spectra of the catalysts, X-ray absorption near edge structure (XANES) and extended X-ray absorption fine structure (EXAFS) were collected on the BL10C beamline at the Pohang Light Source (PLS-II) with a ring current of 100 mA at 3.0 GeV. The monochromatic X-ray beam could be obtained from the high intensity X-ray photons of the multi-pole wiggler source using a liquid nitrogen-cooled Si (111) double crystal monochromator (Bruker ASC). The X-ray absorption spectroscopic data were recorded for the uniformly dispersed powder samples with a proper thickness on the polyimide film, in transmission mode with N_2 gas-filled ionization chambers as detectors. Higher order harmonic contaminations were eliminated by detuning to reduce the incident X-ray intensity by ~40%. Energy calibration was simultaneously carried out for each measurement with a reference metal foil placed in front of the third ion chamber. The data reductions of the experimental spectra to normalized XANES and Fourier-transformed radial distribution function (RDF) were performed through the standard XAFS procedure.

4. Density functional theory calculations

Spin-polarized DFT calculations were carried out using the Vienna ab initio simulation package (VASP)[S4,S5] with projector augmented wave (PAW) [S6] potentials and the revised Perdew-Burke-Ernzerhof (RPBE) exchange-correlation functional[S7]. A 415-eV kinetic energy cut-off for the plane wave basis set was used with Monkhorst-Pack[S8] mesh **k**-points of (3 × 3 × 3) and (3 × 3 × 1) for bulk and surface calculations, respectively, allowing convergence to 0.01 eV of the total electronic energy. We calculated the binding energy of atomic oxygen (BO) as a descriptor for scaling the ORR activity [S9]. Here, BO is defined as BO = E[2O/surface] − E[surface] − 2E[O], where E[2O/surface], E[surface], and E[O], respectively, are the calculated electronic energies of two adsorbed oxygen atoms on a surface, a clean surface, and a triplet oxygen atom, respectively. The calculated equilibrium lattice constant for Pt is 3.998 Å. Since the models of the FeCo-OMPC catalyst (Supplementary Fig.

S16) have two metal centres, we placed an O atom on each metal centre. After optimization, the BOs were averaged in units of eV/atom. Accordingly, the BOs on a five-layer p(2 × 2) Pt(111) surface were also computed at 0.5 monolayer (ML) by placing two O atoms at hollow centres, and they were also averaged. The surface calculations were first carried out on a C, N, and M-terminated (0001) plane (48 C, 16 N, 18 O, 4 M, and 4 H atoms) based on **Model IV**-like bulk structure with a vacuum space of 10 Å. In this case, the surfaces (a 2-bilayer M-OMPC surface) were fixed, while only the adsorbates (2 O atoms) were fully relaxed. Then **Model II** (120 C, 12 N, 18 O, 4 M, and 2 H atoms) was used to generate a C, N, Fe, Co-terminated (0001) surface. For these calculations, the bottom bilayer of the 2-layer FeCo-OMPC surface was fixed, and the top bi-layer and the adsorbates were fully relaxed. For Pt(111), only two topmost layers and the adsorbates were fully relaxed.

5. Electrochemical characterisation

Calibration to reversible hydrogen electrode

The reference electrode was calibrated and reported to a reversible hydrogen electrode (RHE). The RHE calibration was performed in a H_2-saturated electrolyte with platinum wire as the working electrode. The potential was swept near the thermodynamic potential for the H^+/H_2 reaction. The potential at which the current crossed zero was taken to be the potential for this reaction.

Media	Electrolyte	Reference electrode	Thermodynamic potential for hydrogen electrode	Conversion equation
Acid	0.1 M $HClO_4$	Ag/AgCl	-0.268 V vs Ag/AgCl	E(RHE)= E(Ag/AgCl)+0.268 V
Base	0.1 M KOH	Hg/HgO	-0.915 V vs Hg/HgO	E(RHE)=E(Hg/HgO)+0.915 V

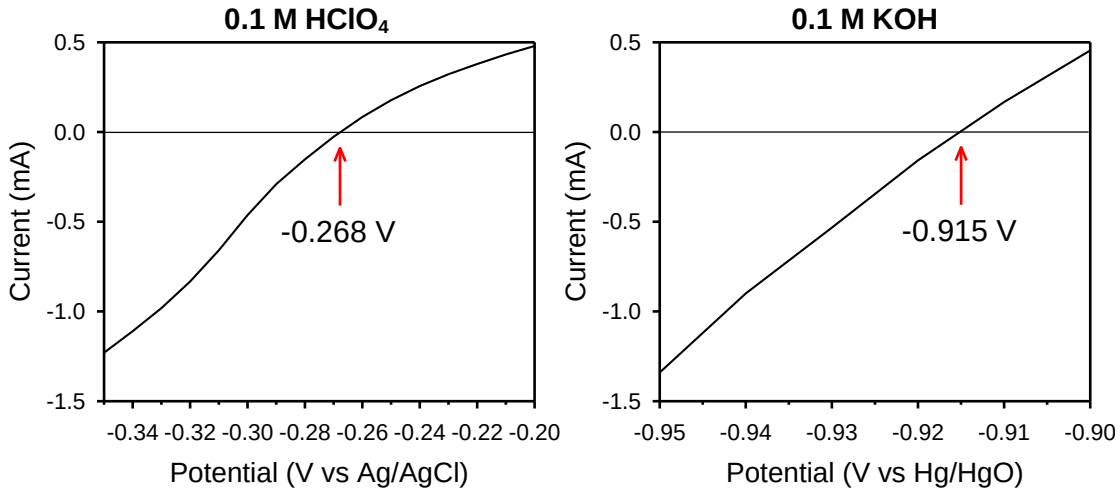

Rotating ring-disk electrode measurements

The rotating ring-disk electrode (RRDE) measurements were used to determine the ORR activity and four-electron selectivity of catalysts. ORR activity was recorded in O_2-saturated 0.1 M $HClO_4$ electrolyte with linear sweep voltammetry (LSV) performed for voltages ranging from 1.1 to 0.2 V at a scan rate of 5 mV s^{-1}. The disk rotation speed was controlled from 100 to 2500 rpm. In the RRDE experiments, the ring potential was set to 1.2 V. The transferred electron number (n) was evaluated based on the RRDE measurements, calculated from the following equation.

$$n = \frac{4}{1 + \frac{I_R}{N I_D}}$$

Here, I_D and I_R are the disk and ring currents, respectively, and N is the ring collection efficiency (44%).

6. PEFC single cell tests

Preparation of catalyst layers

The anode catalyst ink was prepared by mixing commercial Pt supported on graphitized carbon (60 wt%, Johnson Matthey), 2-propanol, DI water, and a Nafion® DE 521 solution (5 wt% Nafion®, 45 ± 3 wt% water, 48 ± 3 wt% 1-propanol, <4 wt% ethanol, and ion exchange capacity (IEC) of 0.95–1.03 meq g^{-1}, DuPont). The ionomer-to-Pt/C ratio was 0.429. The anode catalyst layer with a uniform thickness of 7.5 μm was prepared by a decal process using the following methods: 1) the anode ink was coated onto a decal substrate by a doctor blade film applicator; 2) the catalyst-coated film was dried at room temperature for 2 d; and 3) the catalyst film was hot-pressed on a 50 μm-thick Nafion® 212 membrane (DuPont) at 100 kgf cm^{-2} and 140 °C for 2 min. The anode Pt loading was 0.42 mg_{Pt} cm^{-2}.

The cathode catalyst ink was formulated with catalyst (0.9 g) and Nafion® DE 521 (11.268 g). The ionomer-to-catalyst ratio was 0.626. The cathode catalyst layer with an active area of 25 cm^2 was fabricated by the spray method on the other side of the anode catalyst-coated Nafion® 212 membrane at 80 °C. The targeted catalyst loading was 1.52 mg cm^{-2}. Immediately thereafter, the resulting membrane electrode assemblies (MEAs) were hot-pressed at 400 kgf cm^{-2} and 140 °C for 2 min, producing a cathode catalyst layer with a thickness of about 27 μm.

PEFC single cell test

The H_2 and O_2 gases were humidified by passing them through bubbler-type humidifiers. Before starting the single cell operation, the humidifiers were calibrated using a humidity sensor (Viasensor HS-1000). All single cell experiments were conducted at 80 °C, and the temperature of the gas lines to the anode and the cathode were always set above the temperature of the humidifier by 10 °C to avoid the condensation of the water vapour. The anode was fed with fully humidified H_2 gas at a constant flow rate of 350 mL min^{-1}, and the cathode was fed with fully humidified O_2 gas at a constant flow rate of 2000 mL min^{-1} at 2 bar (gauge pressure) on both sides. The partial pressures of the H_2 and O_2 gases were 1.53 bar because the saturated vapour pressure of water at 80 °C was approximately 0.47 bar. After the

open circuit voltage was stabilized, the polarization curves of the prepared MEAs were obtained at a scan rate of 0.5 mV s^{-1} from OCV to 0.1 V. Electrochemical impedance spectroscopy (EIS) measurements were conducted using an HCP-803 analyser (Bio-Logic Science Instruments). All EIS spectra were obtained under the same operating conditions used to obtain the high frequency resistance-corrected polarization curve. EIS were obtained in constant-current mode by sweeping frequencies over the range 2–150 kHz. The stability measurements of the prepared MEAs were performed at a constant voltage of 0.5 V for 100 h.

Supplementary Table S1. Structural properties of prepared catalysts.

Catalysts	S_{BET} (m^2 g^{-1})[a]	V_{tot} (cm^3 g^{-1})[b]	d_{meso} (nm)[c]
FeCo-OMPC	1190	1.40	4.85
Fe-OMPC	1168	1.49	4.27
Co-OMPC	1112	1.35	4.27
FeCo-OMPC (L)	930	1.65	18.5
FeCo-OMPC (C)	1182	1.02	3.33
OMPC	1496	1.76	4.27
FeCo-KB	105	0.79	3.33
FeCo-Cabosil	546	1.15	10.77

[a] BET specific surface areas obtained from N_2 adsorption isotherm in the range of p/p_0 = 0.05-0.2.
[b] Total pore volumes.
[c] Primary mesopore diameter calculated from BJH method.

Supplementary Table S2. Half-wave potentials and kinetic current densities at 0.9 V of FeCo-OMPC catalysts from 30 different sample batches in 0.1 M $HClO_4$ solution at a scan rate of 5 mV s^{-1}.

Sample batch number	Half-wave potential (V)	Kinetic current density at 0.9 V (mA cm^{-2})
1	0.852	2.44
2	0.845	2.36
3	0.842	2.24
4	0.865	2.81
5	0.86	2.63
6	0.846	2.38
7	0.843	2.33
8	0.851	2.41
9	0.848	2.39
10	0.853	2.48
11	0.851	2.44
12	0.854	2.49
13	0.847	2.37
14	0.844	2.29
15	0.849	2.34
16	0.852	2.4
17	0.855	2.53
18	0.850	2.36
19	0.843	2.28
20	0.847	2.31
21	0.856	2.5
22	0.859	2.57
23	0.861	2.61
24	0.853	2.44
25	0.849	2.38
26	0.855	2.49
27	0.857	2.48
28	0.848	2.33
29	0.845	2.26
30	0.851	2.37
Average	**0.851**	**2.42**
Standard Deviation (%)	**0.68**	**5.07**

Supplementary Table S3. Comparison of half-wave potentials ($E_{1/2}$), kinetic currents (i_k) at 0.9 V and 0.8 V, and mass activity at 0.8 V of the FeCo-OMPC catalyst with previously reported catalysts.

Catalysts	$E_{1/2}$ (V vs RHE)	i_k (@ 0.9 V)[a] (mA cm^{-2})	i_k (@ 0.8 V)[b] (mA cm^{-2})	$i_{k,m}$ (@ 0.8 V)[c] (A g^{-1})	Ref.
FeCo-OMPC This study	**0.851**	**2.42**	**27**	**45**[k]	**This study**
20 wt% Pt/C This study	0.865	2.08	-	-	This study
FeAc-FB[d] Jaouen and Dodelet	-	-	2.5	3.1[l]	S10
FeTMPP-FeO_x[e]-S Jaouen *et al.*	0.810	-	8.3	18[l]	S11
CoTMPP-FeO_x-S Jaouen *et al.*	0.790	-	4.6	10[l]	S11
FeAC-FB[d] Jaouen *et al.*	0.780	-	3.6	4.5[l]	S11
FeAc-PTCDA-BP[f] Jaouen *et al.*	0.760	-	2.4	3[l]	S11
FeAc-Phen-BP[f] Meng *et al.*	0.800	-	16	20[k]	S12
$FeSO_4$-PANI-KB[g] Chlistunoff	0.760	-	1.0	2.0[m]	S13
$FeCl_3$-$Co(NO_3)_2$-HDA-KB[g] Wu *et al.*	0.780	-	5.0	8.4[m]	S14
$FeCl_3$-PANI-KB[g] Wu *et al.*	0.810	-	5.8	3.5[m]	S15
$Fe(NO_3)_3$-NT-G[h] Li *et al.*	0.760	-	2.1	4.4[m]	S16
FeIM-ZIF-8[i] Zhao *et al.*	0.755	-	1.0	2.6[k]	S17
Co-Corrole-CB[j] *Huang et al.*	0.750	-	2.6	-	S18

All data collected from RDE measurements in acidic conditions.
[a] Mass transfer corrected kinetic current per geometric surface area of disk (kinetic current density) at 0.9 V
[b] Kinetic current density at 0.8 V
[c] Kinetic current per catalyst mass at 0.8 V
[d] Furnace black, [e] Fe oxalate, [f] Black Pearl, [g] Ketjen Black, [h] Nanotube-graphene complex, [i] Fe imidazolate and zeolitic imidazolate frameworks, [j] Carbon Black, [k] 0.1 M $HClO_4$, [l] pH 1 H_2SO_4, [m] 0.5 M H_2SO_4.

Supplementary Table S4. Half-wave potentials and kinetic current densities at 0.9 V of FeCo-OMPC and Pt/C catalysts for ORR in 0.1 M $HClO_4$ solution at a scan rate of 1 mV s^{-1}.

	Half-wave potential (V)	**Kinetic current density at 0.9 V (mA cm^{-2})**
FeCo-OMPC	**0.845**	**1.80**
Pt/C	0.840	1.00

Supplementary Table S5. The structural parameters obtained from EXAFS curve-fitting process for the Fe and Co K-edge k^2-weighted EXAFS spectra of the FeCo-OMPC catalyst.

Edge	Path	ΔE (eV)[a]	N[b]	R (Å)[c]	σ^2 ($x10^{-3}$ Å^2)[d]
Fe K-edge	Fe – $O_{1/axial}$	-3.08	1.67	1.88	3.38
	Fe – N_{eq}	1.68	2.83	2.01	4.65
	Fe – $O_{2/axial}$	-8.35	1.96	2.43	2.93
	Fe – C1(5-membered ring)	-9.28	1.68	2.56	2.97
	Fe – C2(6-membered ring)	-6.67	3.42	2.95	7.39
	Fe – C3	3.08	2.42	3.69	5.07
	Fe – $O_{12/axial}$ – Fe	1.76	0.93	4.78	4.91
Co K-edge	Co – $O_{1/axial}$	-7.68	1.05	1.87	2.64
	Co – N_{eq}	-0.18	2.29	1.94	4.08
	Co – C1 (or C2)	-2.08	1.80	2.89	1.81
	Co – $O_{12/axial}$ – Co(1)	5.77	0.62	4.46	8.94
	Co – $O_{12/axial}$ – Co(2)	9.25	0.27	4.85	7.44

[a] Energy shift.
[b] Coordination number.
[c] Bond distance.
[d] Debye-Waller factor for each scattering path.

Supplementary Table S6. Binding of oxygen (BO) on the surfaces using the **Model IV** and **Model II** bulk structures.

Model IV[a]	Fe-OMPC	Co-OMPC	FeCo-OMPC	Pt(111)[a]
BO (eV/atom)	–4.94	–4.02	–3.14	–3.47
Model II[b]	Fe-OMPC	Co-OMPC	FeCo-OMPC	Pt(111)[c]
BO (eV/atom)	–	–	–3.33	–3.58

[a] The surfaces were fixed and only the adsorbates were fully relaxed.
[b] The bottom bilayer was fixed, and the top bilayer and the adsorbates were fully relaxed.
[c] The topmost two layers and the adsorbates were fully relaxed, while the bottom three layers were fixed.

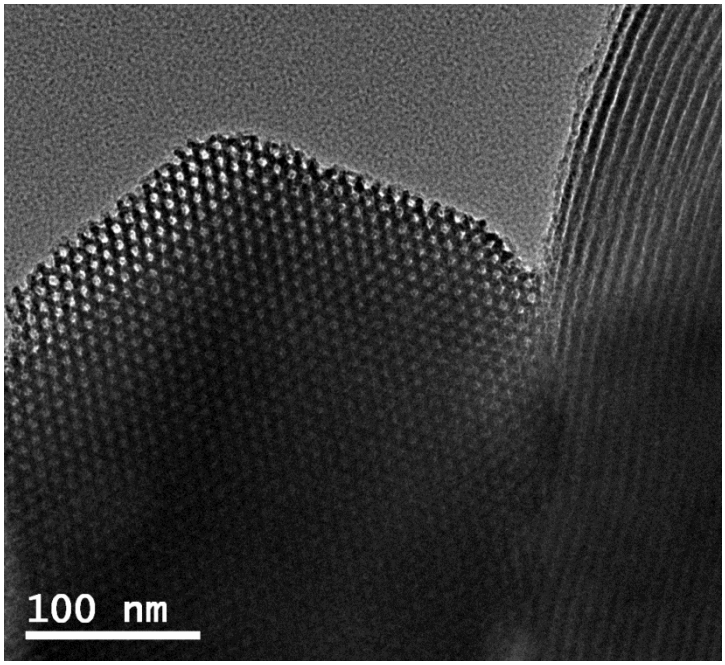

Supplementary Figure S1. TEM image of SBA-15 mesoporous silica template.

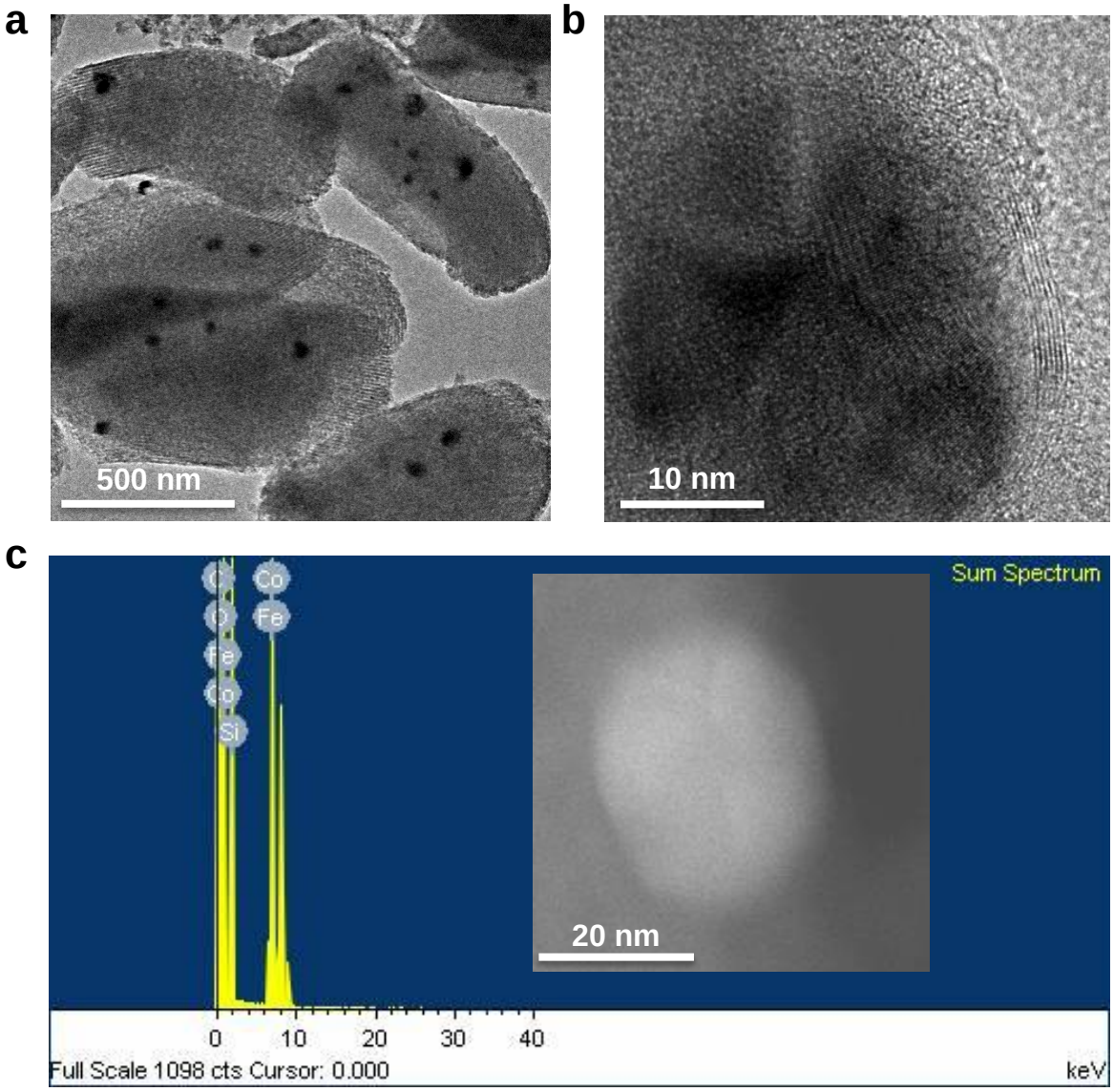

Supplementary Figure S2. TEM and EDX characterisation of carbon/SBA-15 composite during the synthesis of the FeCo-OMPC catalyst. (a) TEM image of carbon/SBA-15 particles. (b) High-resolution TEM image of a single FeCo particle. (c) EDX analysis over a single FeCo particle.

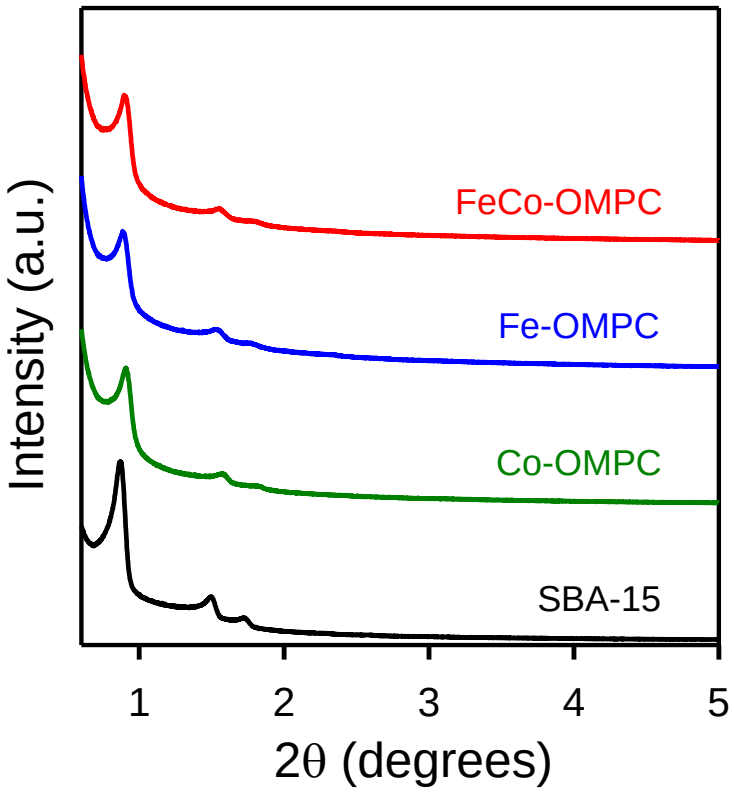

Supplementary Figure S3. Low-angle XRD patterns of SBA-15 and M-OMPC catalysts.

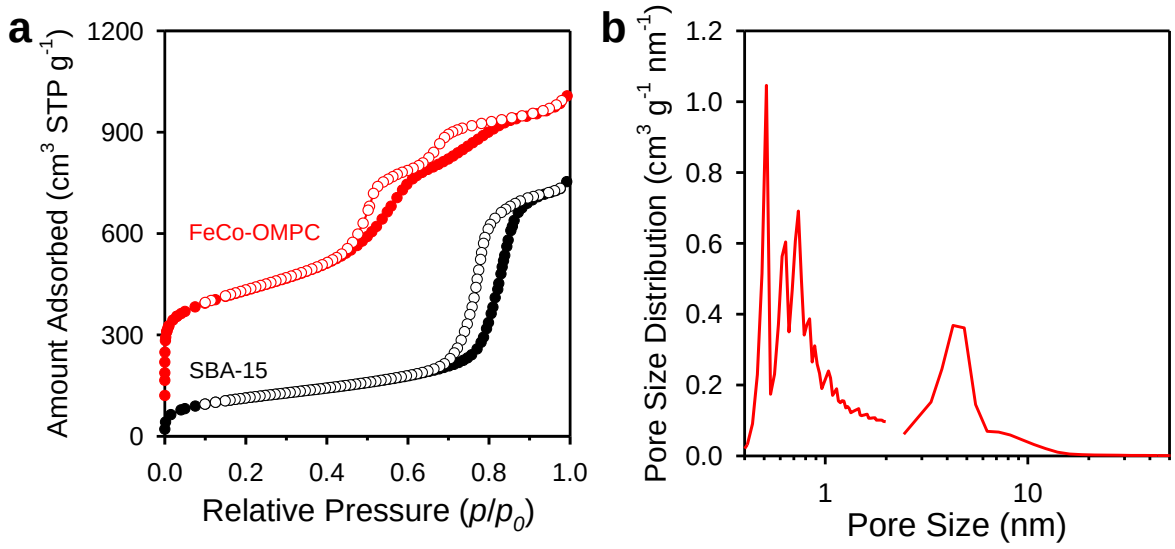

Supplementary Figure S4. (a) N_2 adsorption isotherms of SBA-15 template and FeCo-OMPC catalyst. (b) The pore size distribution curve of FeCo-OMPC obtained from adsorption branch of its isotherm.

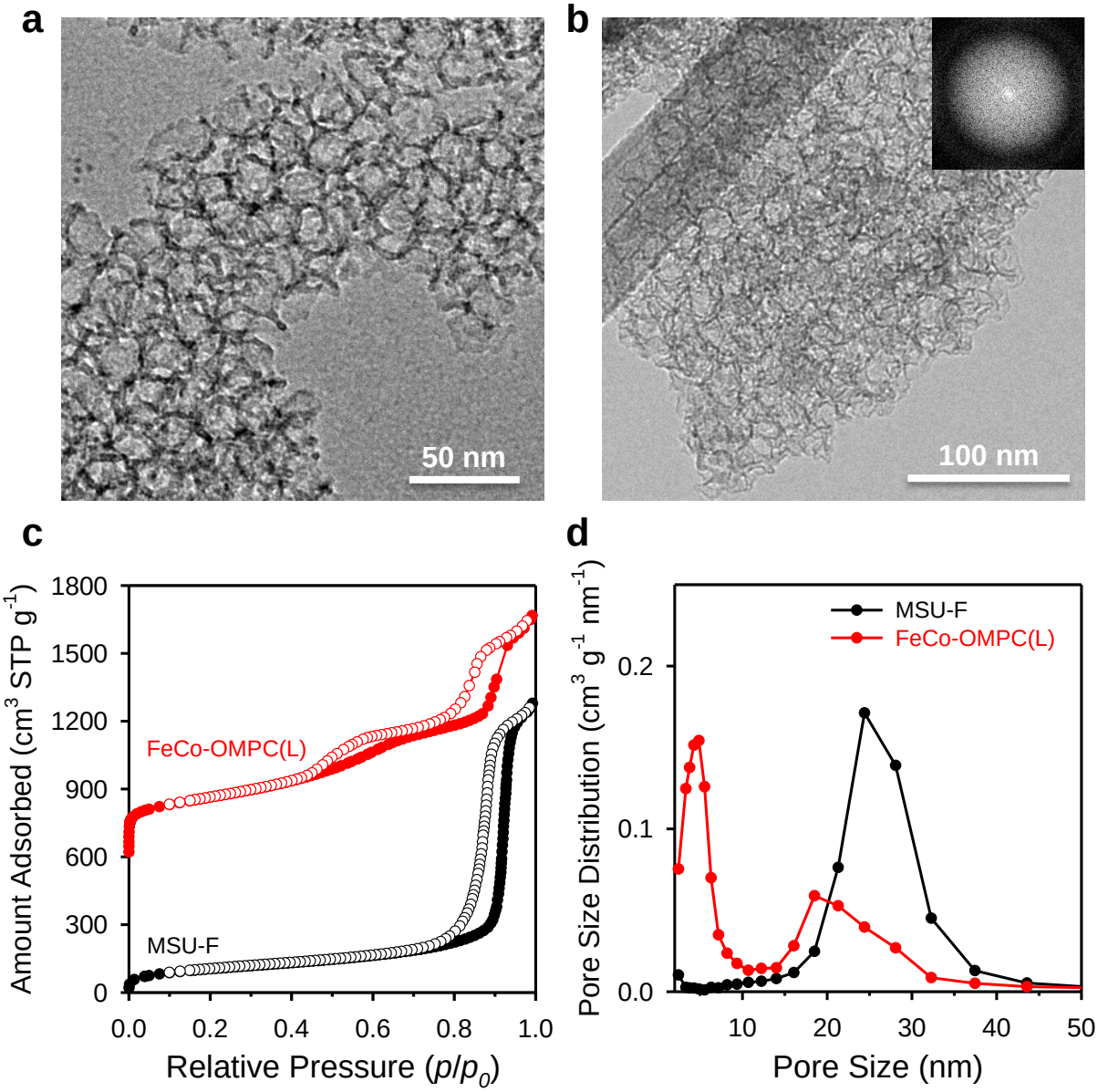

Supplementary Figure S5. Structural characterisation of MSU-F silica and FeCo-OMPC(L). (a) TEM image of large pore MSU-F mesoporous silica template. (b) TEM image and the corresponding Fourier diffractogram (inset) of large pore FeCo-OMPC(L) templated from MSU-F mesoporous silica. (c) N_2 adsorption isotherms of MSU-F mesoporous silica template and FeCo-OMPC(L) catalyst. (d) The corresponding pore size distribution curves obtained from adsorption branches of their isotherms. The isotherm of FeCo-OMPC(L) is shifted 600 cm^3 g^{-1} upwards for clarity.

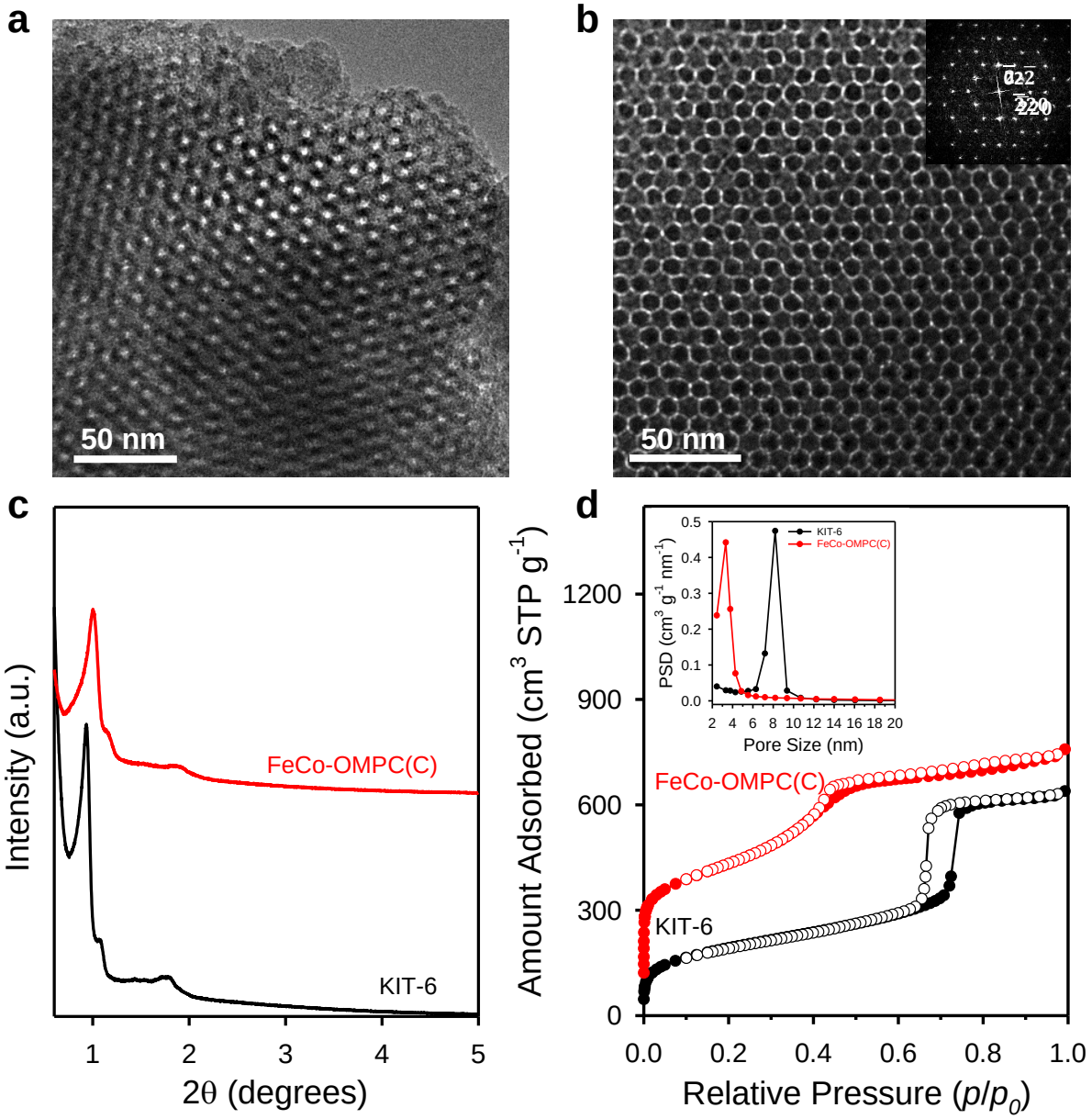

Supplementary Figure S6. Structural characterisation of metal-free OMPC. (a) TEM images of KIT-6 mesoporous silica template with cubic *Ia3d* mesostructure. (b) TEM image and the corresponding Fourier diffractogram (inset) of cubic *Ia3d* type FeCo-OMPC(C) catalyst templated from KIT-6 mesoporous silica. (c) Low-angle XRD patterns. (d) N_2 adsorption isotherms of KIT-6 mesoporous silica template and FeCo-OMPC(C) catalyst and the corresponding pore size distribution curves (inset) obtained from adsorption branches of their isotherms. The isotherm of FeCo-OMPC(C) catalyst was shifted 100 cm^3 g^{-1} upwards for clarity.

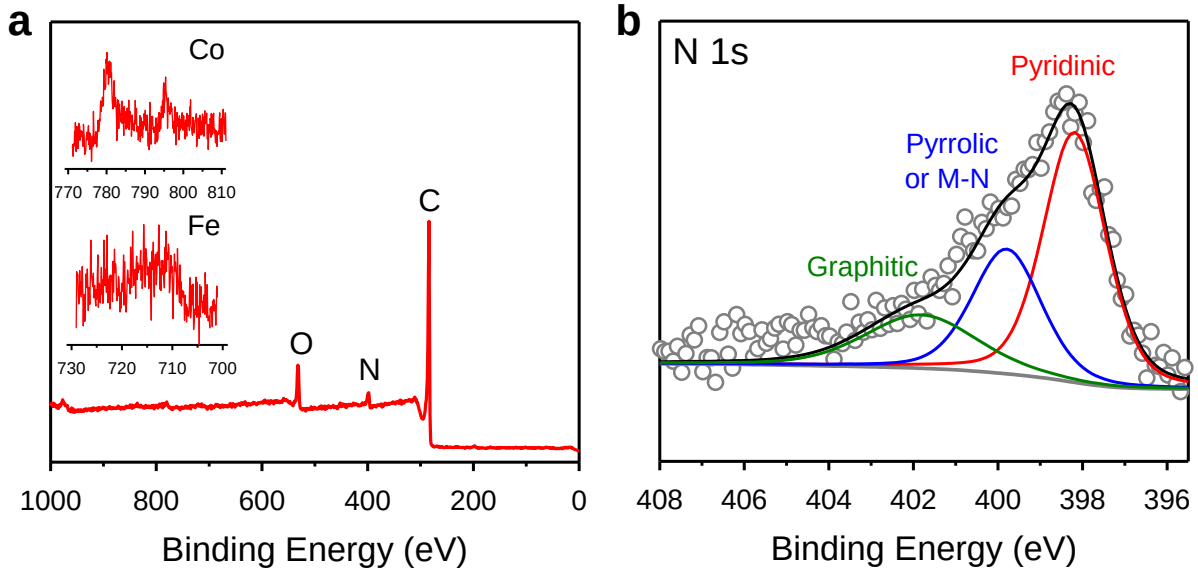

Supplementary Figure S7. XPS survey (a) and N 1s spectra (b) of FeCo-OMPC catalyst.

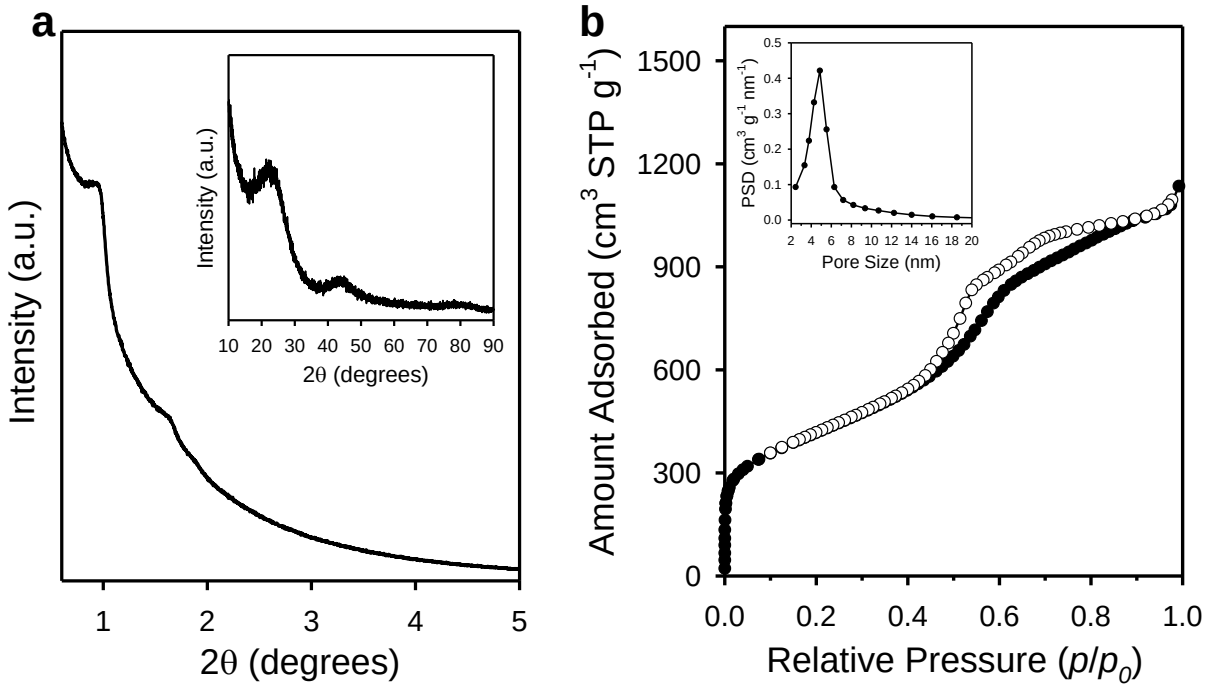

Supplementary Figure S8. Structural characterisation of metal-free OMPC. (a) Low-angle and wide-angle XRD pattern (inset). (b) N_2 adsorption isotherm and the corresponding pore size distribution curve (inset) obtained from adsorption branch of the isotherm.

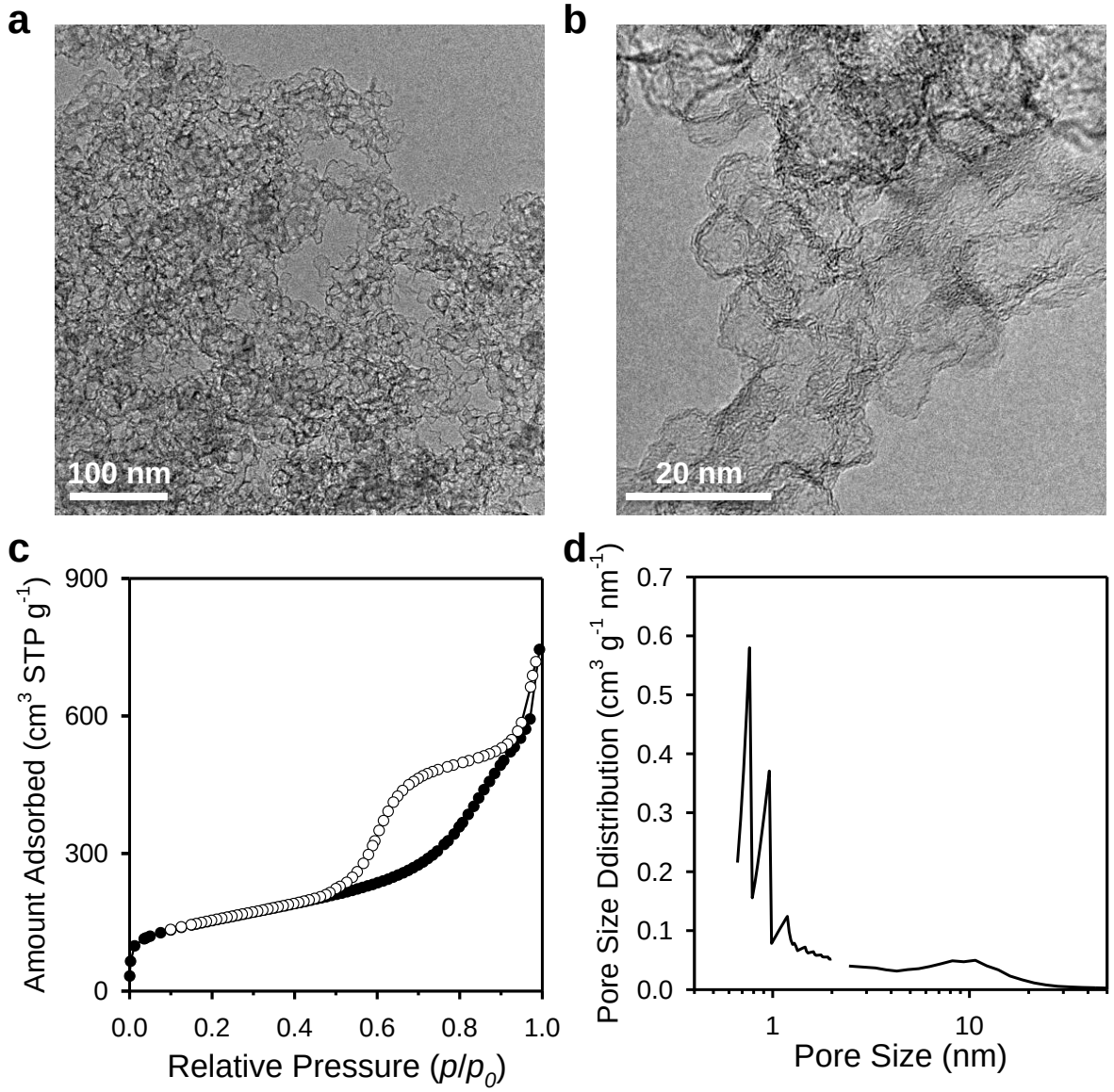

Supplementary Figure S9. Structural characterisation of FeCo-OMPC. (a,b) TEM images. (c) N_2 adsorption isotherm and (d) the corresponding pore size distribution curve from adsorption branch obtained from adsorption branch of the isotherm.

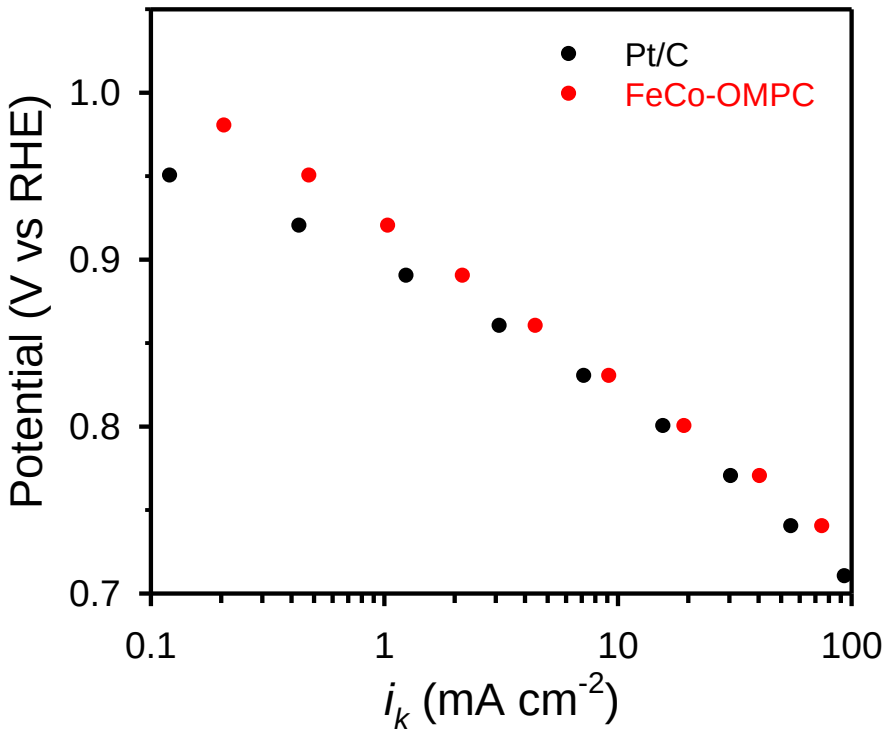

Supplementary Figure S10. Tafel plots of Pt/C and FeCo-OMPC catalysts obtained from ORR polarisation curves measured at a scan rate of 1 mV s^{-1}.

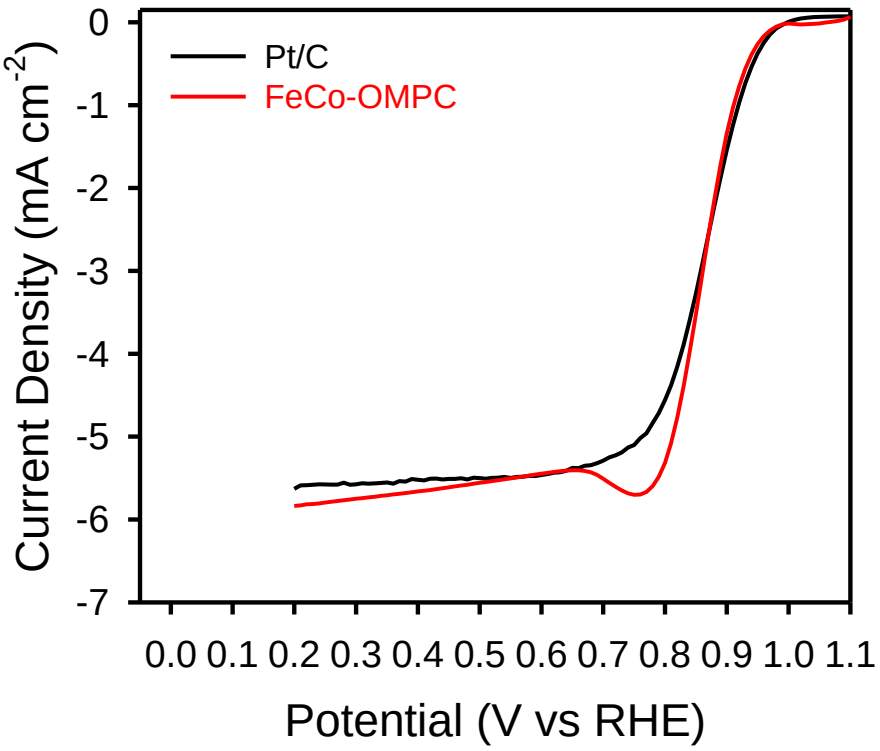

Supplementary Figure S11. ORR polarisation curves of Pt/C and FeCo-OMPC catalysts in O_2-saturated 0.1 M KOH. The catalyst loadings were 0.3 mg cm^{-2} for the FeCo-OMPC catalysts and 20 μg_{Pt} cm^{-2} for Pt/C. The electrode rotation speed was 1600 rpm and the scan rate was 5 mV s^{-1}.

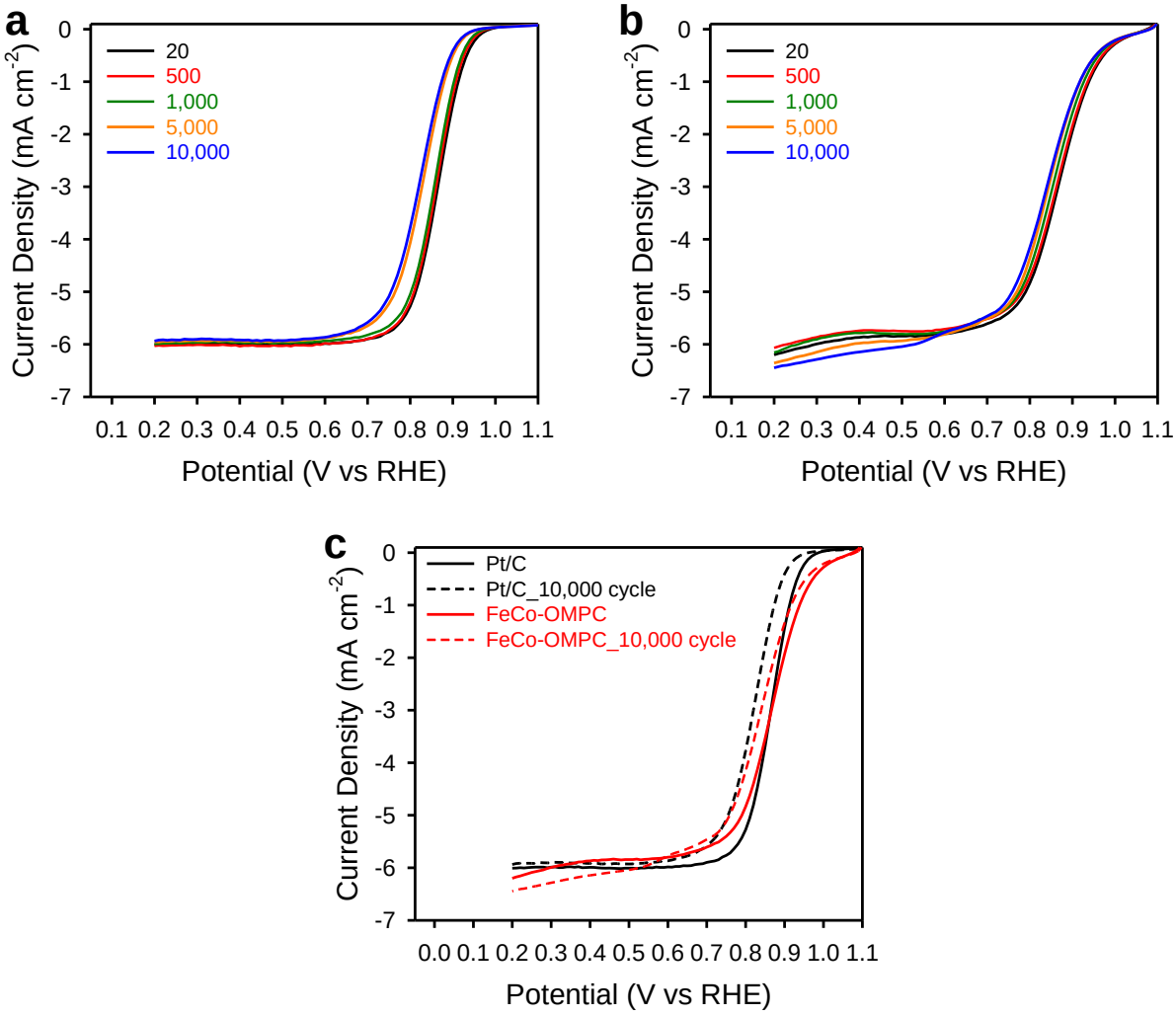

Supplementary Figure S12. Evolution of ORR polarisation curves of Pt/C (a) and FeCo-OMPC (b) catalysts under the potential cycling in N_2 saturated 0.1 M $HClO_4$. (c) ORR polarization curves of Pt/C and FeCo-OMPC catalysts before and after 10,000 potential cycles in N_2-saturated 0.1 M $HClO_4$.

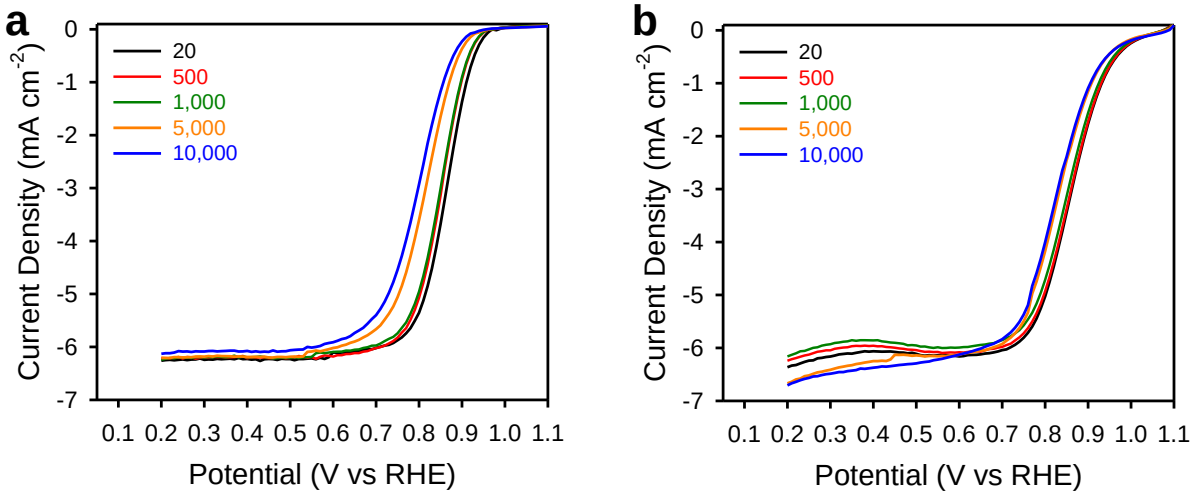

Supplementary Figure S13. Evolution of ORR polarisation curves of (a) Pt/C and (b) FeCo-OMPC catalysts under the potential cycling in O_2 saturated 0.1 M $HClO_4$.

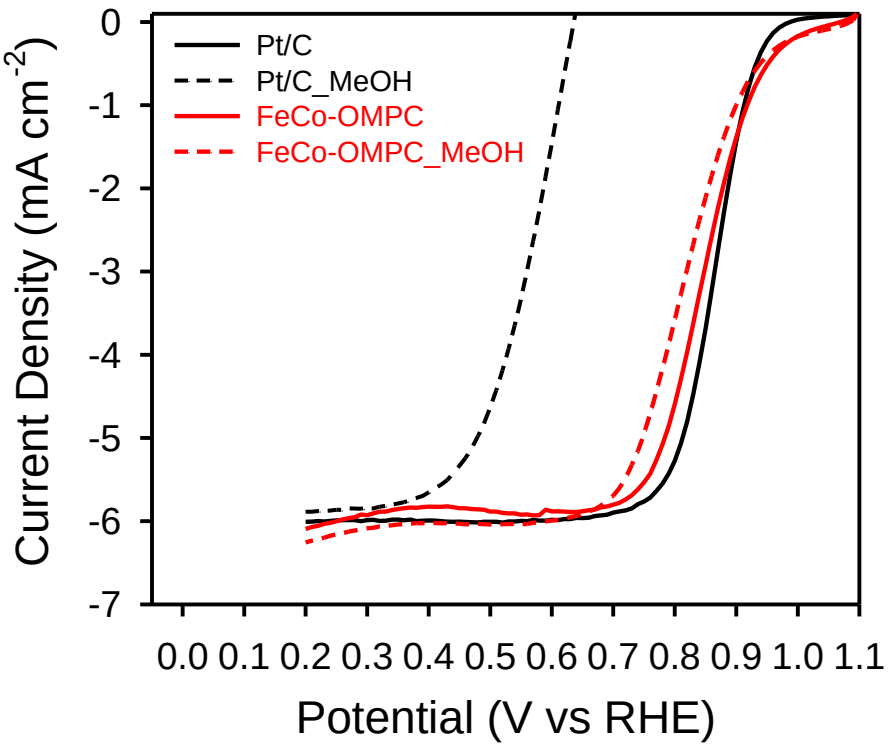

Supplementary Figure S14. ORR polarisation curves of Pt/C and FeCo-OMPC catalysts in O_2-saturated 0.1 M $HClO_4$ with or without 0.5 M methanol. The catalyst loadings were 0.6 mg cm^{-2} for FeCo-OMPC catalyst and 20 μg_{Pt} cm^{-2} for Pt/C. The electrode rotation speed was 1600 rpm and the scan rate was 5 mV s^{-1}.

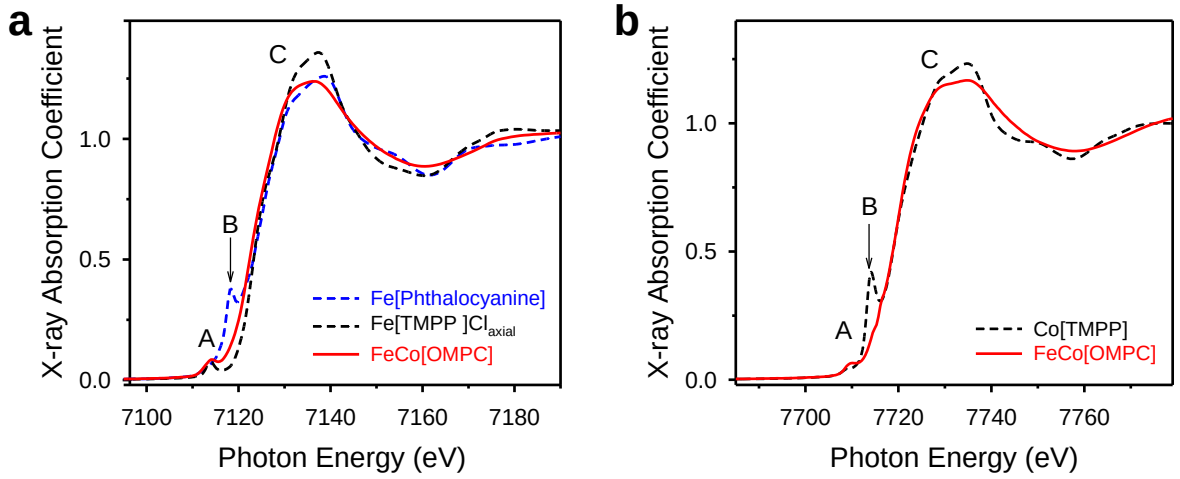

Supplementary Figure S15. (a) Fe and (b) Co K-edge X-ray absorption near edge structures (XANES) spectra of FeCo-OMPC and model compounds.

The reference materials (Fe-phthalocyanine and CoTMPP) with four nitrogen-coordination around each central atom have a distinct shoulder absorption peak (peak B in Fig. S15). The peak B corresponds to electronic-transition to unoccupied $4p_z$ orbital with ligand-to-metal charge transfer process, which is well-known to be characteristic of ligand distribution environment under square-planar (D_{4h}) symmetry. On the other hand, both Fe and Co K-edge XANES spectra of the FeCo-OMPC catalyst present distinct disappearance of the square-planar characteristic peak, which means there is an existence of another ligand-coordination around central atoms followed by the five- or six-ligand coordination.

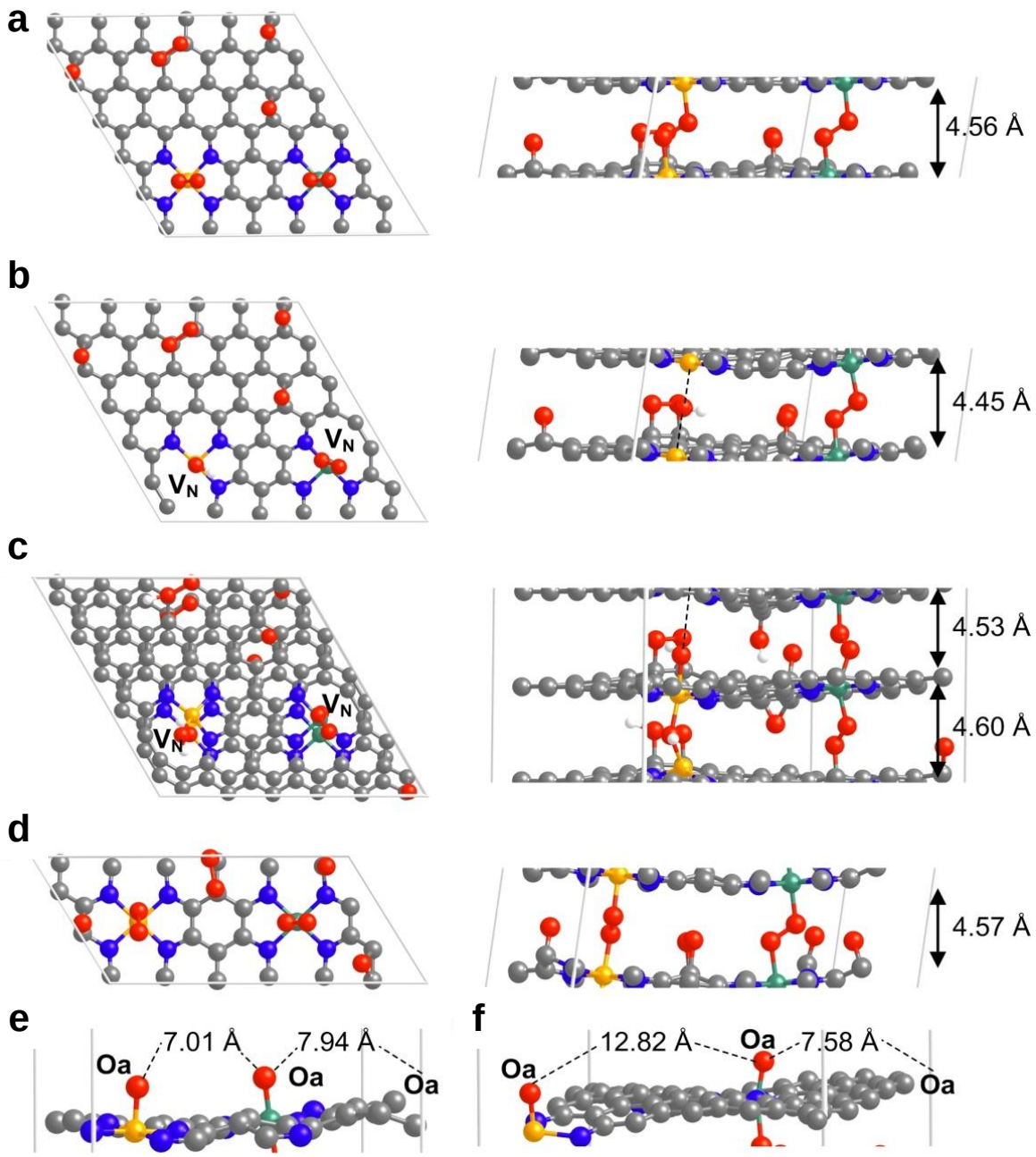
a
4.56 Å
b
V_N
V_N
4.45 Å
c
V_N
V_N
4.53 Å
4.60 Å
d
4.57 Å
e
Oa
7.01 Å
7.94 Å
Oa
Oa
f
Oa
12.82 Å
Oa
7.58 Å
Oa

Supplementary Figure S16. Top and side views of bulk structures (a) **Model I** (60 C, 8 N, 9 O, 1 Fe, and 1 Co atoms), (b) **Model II** (60 C, 6 N, 8 O, 1 Fe, 1 Co, and 1 H atoms), (c) **Model III** (120 C, 12 N, 14 O, 2 Fe, 2 Co, and 2 H atoms), and (d) **Model IV** (24 C, 8 N, 8 O, 1 Fe, 1 Co, and 2 H atoms). **Model I** was first built, and then, **Model II** was prepared by removing two nitrogen atoms, representing nitrogen vacancies ($\mathbf{V_N}$) and by replacing OO bridging Co-Co with OH. To generate $\mathbf{V_N}$, we fully re-optimized the structures by removing nitrogen atoms one by one. Based on **Model II**, **Model III** was constructed. To save the computational time for surface calculations, a simplified bulk structure of **Model IV** was built. **Model I**, **Model II**, and **Model IV** have one layer in the bulk structure, while **Model III** has two layers. Side views of (e) the surface from **Model IV** and (f) that from **Model II** with a vacuum space of 10 Å. For clarity, only the topmost layer was shown. **Oa** represent adsorbed oxygen species. Grey, blue, green, orange, red, and white spheres represent C, N, Fe, Co, O, and H, respectively.

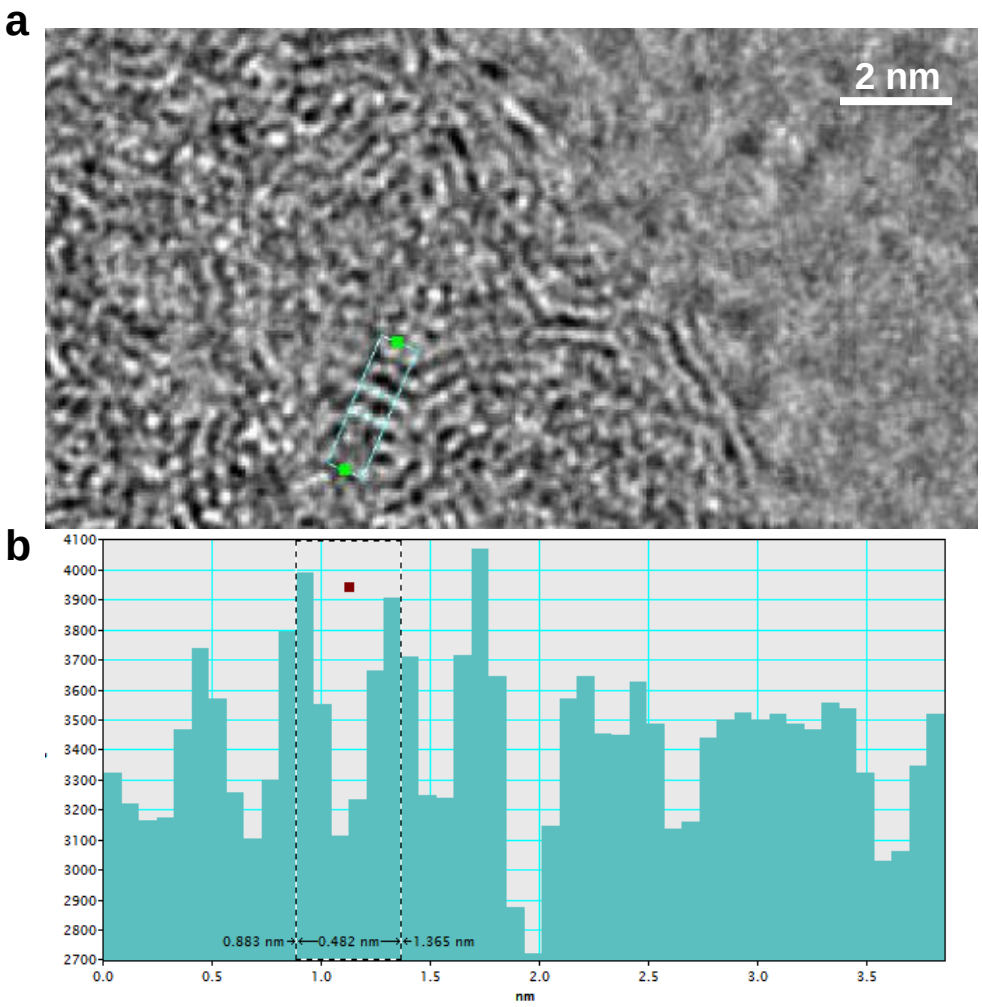

Supplementary Figure S17. (a) HRTEM image of frameworks within FeCo-OMPC catalyst. (b) Interlayer distance between adjacent carbogenic layers. The distance is 0.48 nm.

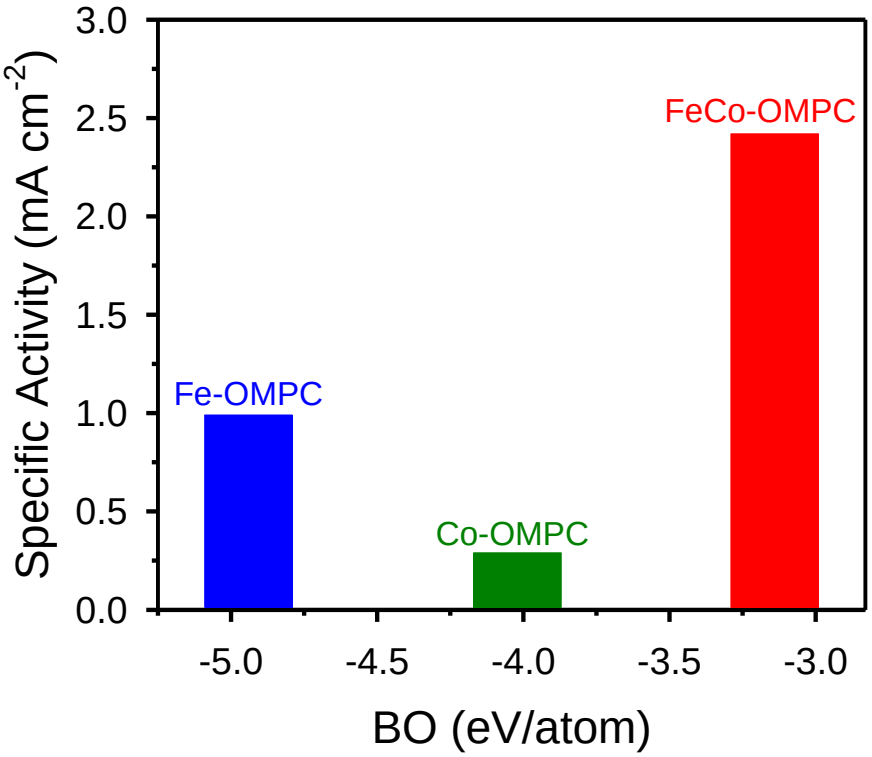

Supplementary Figure S18. Specific activity against binding energy of oxygen atom (BO) over Fe-, Co-, and FeCo-OMPC catalysts using **Model IV**. For these BO calculations, the surfaces were fixed, and only the adsorbed oxygen species were fully optimized. The geometrical parameters are summarized in Table S6.

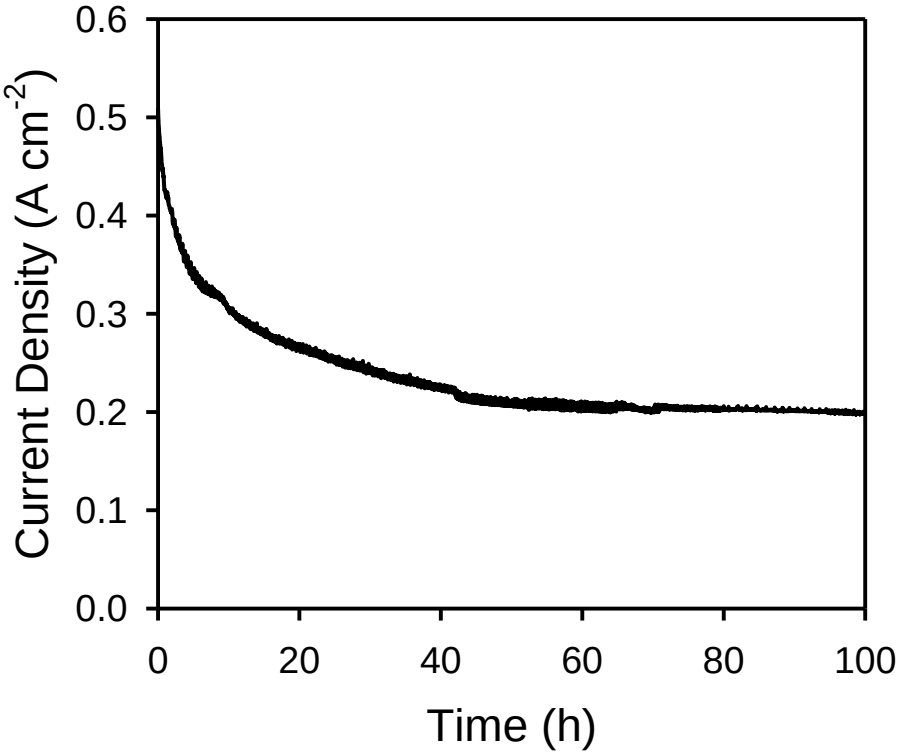

Supplementary Figure S19. Long-term durability test for a PEFC that employed FeCo-OMPC(L) cathode at a constant voltage of 0.5 V operated with H_2-O_2.

References for Supplementary Information

S1. Zhao, D. *et al.* Triblock copolymer syntheses of mesoporous silica with periodic 50 to 300 angstrom pores. *Science* **279**, 548-552 (1998).

S2. Kim, S.-S., Pauly, T. R. & Pinnavaia, T. J. Non-ionic surfactant assembly of ordered, very large pore molecular sieve silicas from water soluble silicates. *Chem. Commun.* 1661-1662 (2000).

S3. Kleitz, F., Choi, S. H. & Ryoo, R. Synthesis of thermally stable mesoporous cerium oxide with nanocrystalline frameworks using mesoporous silica templates. *Chem. Commun.* 2136-2137 (2003).

S4. Kresse, G. & Hafner, J. *Ab initio* molecular dynamics for liquid metals. *Phys. Rev. B* **47**, 558-561 (1993).

S5. Kresse, G. & Furthmuller, J. Efficient iterative schemes for *ab initio* total-energy calculations using a plane-wave basis set. *Phys. Rev. B* **54**, 11169-11186 (1996).

S6. Blöchl, P. E. Projector augmented-wave method. *Phys. Rev. B* **50**, 17953-17979 (1994).

S7. Hammer, B., Hansen, L.B. & Nørskov, J.K. Improved adsorption energetics within density-functional theory using revised Perdew-Burke-Ernzerhof functionals. *Phys. Rev. B* **59**, 7413-7421 (1999).

S8. Monkhorst, H. J. & Pack, J. D. Special points for Brillouin-zone integrations. *Phys. Rev. B* **13**, 5188-5192 (1976).

S9. Kuttiyiel, K. A. *et al*. Bimetallic IrNi core platinum monolayer shell electrocatalysts for the oxygen reduction reaction. *Energy Environ. Sci.* **5**, 5297-5304 (2012).\

S10. Charreteur, F., Jaouen, F. & Dodelet, J.-P. Iron porphyrin-based cathode catalysts for PEM fuel cells: Influence of pyrolysis gas on activity and stability. *Electrochim. Acta* **54**, 6622-6630 (2009).

S11. Jaouen, F. *et al.* Cross-laboratory experimental study of non-noble-metal electrocatalysts for the oxygen reduction reaction. *ACS Appl. Mater. Interfaces* **1**, 1623-1639 (2009).

S12. Meng, H., Jaouen, F., Proietti, E., Lefevre, M. & Dodelet, J.-P. pH-effect on oxygen reduction activity of Fe-based electro-catalysts. *Electrochem. Commun.* **11**, 1986-1989 (2009).

S13. Chlistunoff, J. RRDE and voltammetric study of ORR on pyrolyzed Fe/polyaniline catalyst. On the origins of variable Tafel slopes. *J. Phys. Chem. C* **115**, 6496-6507 (2011).

S14. Wu, G. *et al.* Synthesis of nitrogen-doped onion-like carbon and its use in carbon-based CoFe binary non-precious-metal catalysts for oxygen-reduction. *Carbon* **49**, 3972-3982 (2011).

S15. Wu, G., More, K. L., Johnston, C. M. & Zelenay, P. High-performance electrocatalysts for oxygen reduction derived from polyaniline, iron, and cobalt. *Science* **332**, 443-447 (2011).

S16. Li, Y. *et al.* An oxygen reduction electrocatalyst based on carbon nanotube-graphene complexes. *Nature Nanotech.* **7**, 394-400 (2012).

S17. Zhao, D. *et al.* Iron imidazolate framework as precursor for electrocatalysts in polymer electrolyte membrane fuel cells. *Chem. Sci.* **3**, 3200-3205 (2012).

S18. Huang, H.-C. *et al.* Pyrolyzed cobalt corrole as a potential non-precious catalyst for fuel cells. *Adv. Funct. Mater.* **22**, 3500-3508 (2012).